



Ground Magnetic Surveying and Susceptibility Mapping Across Weathered Basalt Dikes Reveal Soil Creep and Pedoturbation

Tilo von Dobeneck*, Maximilian Müller, Benjamin Bosbach and Andreas Klügel

Faculty of Geosciences, University of Bremen, Bremen, Germany

OPEN ACCESS

Edited by:

Ricardo IF Trindade,
University of São Paulo, Brazil

Reviewed by:

Melina Macouin,
UMR5563 Géosciences
Environnement Toulouse (GET),
France
Antonio Casas,
University of Zaragoza, Spain

*Correspondence:

Tilo von Dobeneck
dobeneck@uni-bremen.de

Specialty section:

This article was submitted to
Geomagnetism and Paleomagnetism,
a section of the journal
Frontiers in Earth Science

Received: 09 August 2020

Accepted: 07 December 2020

Published: 15 January 2021

Citation:

von Dobeneck T, Müller M, Bosbach B
and Klügel A (2021) Ground Magnetic
Surveying and Susceptibility Mapping
Across Weathered Basalt Dikes Reveal
Soil Creep and Pedoturbation.
Front. Earth Sci. 8:592986.
doi: 10.3389/feart.2020.592986

Ground magnetic survey profiles across a soil-covered and weathered mafic dike in sedimentary host rock not only permit to delineate the strike, width and burial depth of the intrusive basalt sheet, but also reflect the subsurface deformation of its clayey weathering products. We illustrate this finding and its practical geomorphological applicability by an example from the mid-German Heldburg Dike Swarm, where blue- and olive-gray basalt-derived clays inherited not just the dike space previously occupied by the basalt, but also large parts of its magnetic iron minerals and their strong induced and remanent magnetization. Such ductile basaltic “marker soils” deform and move with the surrounding low-magnetic host soils, but remain distinguishable by their contrasting colors and high magnetic susceptibility. Ground magnetic surveys can therefore delineate soil creep distance at meter- and basalt weathering depth at decimeter-precision. Magnetic mapping of a weathered dike’s cross-section from an exploration trench by *in-situ* susceptometry permits to analyze past soil deformation in great detail. Weathering and solifluction transforms the simple “vertical sheet” anomalies of dikes into complex, but still interpretable composite patterns, providing a new and promising exploratory approach for field studies concerned with soil creep and pedoturbation.

Keywords: soil creep marker, weathered basalt dikes, magnetic anomaly, ground magnetic survey, *in-situ* susceptometry, Heldburg Dike Swarm

INTRODUCTION

Soil creep and pedoturbation are fundamental issues of geomorphology and pedology (Pawlik and Šamonil, 2018). Patient observations, often over several years, are needed to assess and quantify the slow motion and deformation of soils properly. Biological creep markers such as tree tilting have been occasionally used (e.g., Alestalo, 1971; Gärtner and Heinrich, 2013), but their vertical, lateral and temporal resolution is fairly limited. Geological soil creep markers such as soil-embedded “stone lines” originating from weathering-resistant quartz veins in the underlying bed rock (Johnson, 2002) can potentially delineate the entire creep trajectory of a soil complex from pedogenesis to erosion. However, finding such durable marker rocks in a soil complex and following their spatial dispersal requires fortunate geological settings and massive, meticulous soil excavations. Here, we propose a more rapid and less invasive concept to deduce past soil creep from irregular magnetic anomalies of weathered basalt dikes using established ground magnetic survey and *in-situ* susceptometry methods.

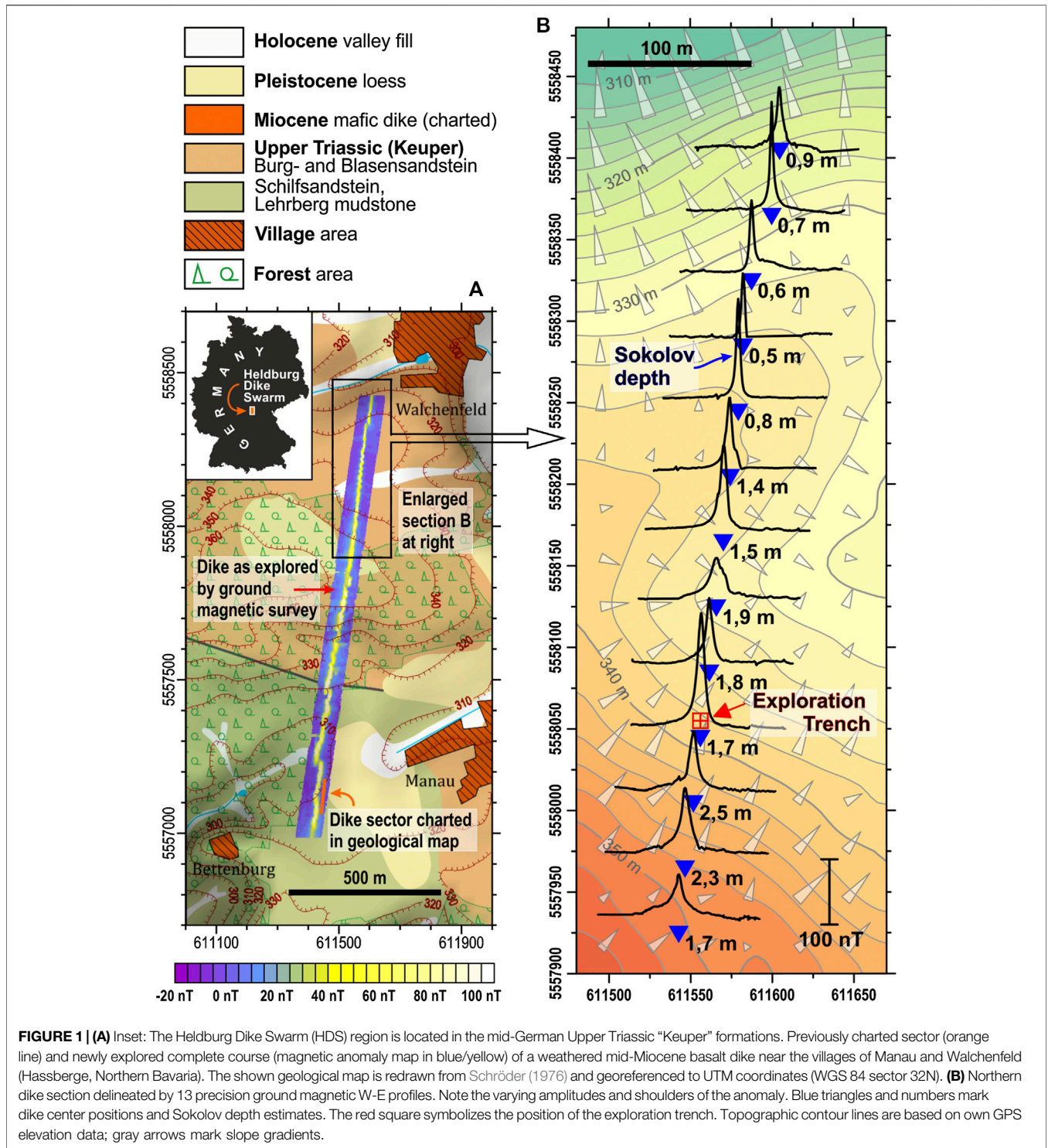


FIGURE 1 | (A) Inset: The Heldburg Dike Swarm (HDS) region is located in the mid-German Upper Triassic “Keuper” formations. Previously charted sector (orange line) and newly explored complete course (magnetic anomaly map in blue/yellow) of a weathered mid-Miocene basalt dike near the villages of Manau and Walchenfeld (Hassberge, Northern Bavaria). The shown geological map is redrawn from Schröder (1976) and georeferenced to UTM coordinates (WGS 84 sector 32N). **(B)** Northern dike section delineated by 13 precision ground magnetic W-E profiles. Note the varying amplitudes and shoulders of the anomaly. Blue triangles and numbers mark dike center positions and Sokolov depth estimates. The red square symbolizes the position of the exploration trench. Topographic contour lines are based on own GPS elevation data; gray arrows mark slope gradients.

GEOLOGICAL SETTINGS

Volcanic dike swarms in sedimentary host rock are typical features of extensional continental basins with underlying small-volume intraplate volcanic fields. We chose the “Heldburg Dike Swarm” (HDS) for our ground magnetic

studies, a 70 × 20 km large mid-German intraplate volcanic field with numerous typically 0.1–10 km long, ~1 m wide, near-vertical basalt dikes, that are parallel with the “Rhenish” NNE-SSW strike of the European Cenozoic Rift System (Wilson and Downes, 2006). The silica-undersaturated basalts of the HDS intruded into the Upper Triassic “Keuper” formations of the

Hassberge cuesta range in Northern Bavaria during early Oligocene and in mid-Miocene (Abratis et al., 2015; Pfänder et al., 2018). Typical local host rocks of HDS dikes are partly dolomitized quartz and arkose sandstones, siltstones and claystones (Geyer and Schmidt-Kaler, 2006).

Owing to intense weathering and solifluction, in particular under past periglacial conditions, these dikes are now concealed under meter-thick soil cover and hard to detect with geological field methods. Their representation in official geological maps is largely incomplete and often oversimplified as **Figure 1A** exemplifies. Finding and tracking hidden mafic dikes is a classical task for ground magnetic surveying. During yearly applied magnetics field courses from 2013 to 2020, Bremen geoscience students have magnetically explored several Bavarian HDS dikes in full length and high resolution. As the basalt's strong magnetization highly contrasts with the low magnetizations of the sedimentary host rocks and soils, the magnetic anomalies of clay-weathered HDS dikes emerge prominently from the very quiet magnetic background of the Keuper formations. We present as our case study a so far largely unknown buried dike near the Franconian villages of Manau and Walchenfeld, whose course through hilly forest- and farmland is clearly delineated by its magnetic anomaly (**Figure 1A**).

METHODS

Ground Magnetic Surveying and Data Processing

During two four-days campaigns in 2015 and 2018, we surveyed the total magnetic field $B(x, y)$ and its vertical gradient $dB/dz(x, y)$ over a parallelogram-shaped area enclosing the Manau-Walchenfeld dike using three portable *GEM GSM-19GW* Overhauser gradiometers as “rovers” and a fourth *GEM GSM-19* as “base.” The lower of the rover's two Overhauser sensors (whose data are shown here) was attached to a vertical aluminum pole such that it was always held or carried 0.7 m above ground. The upper (gradiometer) sensor was mounted in 1.7 m and the GPS antenna in 2.5 m height. Starting from a short previously known dike section (orange line in **Figure 1A**), the dike's course and full length (~1.5 km) was first determined by zigzagging GPS-guided exploratory search profiles. The entire dike was then surveyed in great detail along some 130 parallel ground magnetic W-E lines of 200 m (2015) or 100 m (2018) length, mutually offset by 20 m in the southern sector (lower part of **Figure 1A**) and by 8 m in the northern sector (**Figure 1B**).

Every fifth survey line was measured in the more precise “point mode,” where the magnetometer was manually placed on an oriented surveyor's ribbon in 50 cm steps (exploration trench profile: 25 cm) and readings were averaged over 3 s sampling time. This more time-consuming method enabled us to obtain ± 1 nT data repeatability and an estimated relative positioning error of $\Delta x \leq 10$ cm required for dependable numerical anomaly modeling. The other four out of five intermediary survey lines were surveyed in the faster “walking mode,” where the operator carried the two sensors on a non-magnetic backpack along staked-out ranging rod lines. Walking at a speed of ~ 1 m/s,

the chosen sampling time of 0.5 s is equivalent to ~ 0.5 m data spacing. On open farmland, walking mode data have a dynamic GPS positioning error of about ± 1 m, which is acceptable for mapping purposes. In densely forested areas, an intolerable GPS error of up to ± 5 m forced us to partly return to traditional, more laborious surveying methods based on ranging rods, surveyor's ribbon and compass for profile setup.

Data processing and numerical 2D forward modeling were conducted with *Geosoft Oasis montaj* software. All ground magnetic data were corrected for diurnal field variation using own base station recordings and levelled to remove heading error. Anthropogenic structures like roads, wire fences or signposts were charted and their assumed anomalies eliminated from profiles. An averaged regional geomagnetic background field was subtracted from all survey profiles; an additional linear regional trend correction was applied to the modeled profile.

Exploration Trench and *In-Situ* Susceptometry

In order to reveal the geometry and weathering state and to determine the paleo- and rock magnetic properties of the buried dike structure, an approximately 2.50 m long, 0.80 m wide and 1.80 m deep exploration trench was dug across the anomaly center in a hillslope location (marked in **Figure 1B**) and extended sideways by auger drill soil probing. The near-vertical northern trench wall was subdivided into 5×7 sectors of 50×25 cm size with pegs and strings, that were individually photographed (photo mosaic in **Figure 2A**), visually described (with finger probe), and magnetically mapped using a battery-powered *Bartington MS2F* susceptometer with point sensor, whose sampling time was set to 10 or 1 s depending on the required sensitivity range. A stencil with 50 holes on a 5×5 cm grid was attached to each trench wall sector to facilitate a quick and accurate sequential placement of the point sensor to all $50 \times 37 = 1850$ susceptibility grid positions on the trench wall (**Figure 2B**).

Paleo- and Rock Magnetic Sampling and Laboratory Measurements

To obtain calibrated volume susceptibility (κ) and Natural Remanent Magnetization (NRM) values for all observed materials, required for subsequent numerical anomaly modeling, 106 paleomagnetic sample cubes of 6.2 cm^3 volume were pressed into the trench wall along three vertical transects to collect host soils and different basalt weathering stages. Some soil-embedded basalt relicts of the local dike and from pristine nearby basalt outcrops were likewise fixated in sample cubes. Volume susceptibility measurements of all collected cube samples were taken with a *Kappabridge KLY-2* precision susceptometer. NRM intensity and orientation were determined with the automated *2G 755R* cryogenic DC SQUID magnetometer of our paleomagnetic laboratory (Mullender et al., 2016). The remanent (M_{rem}) and induced (M_{ind}) magnetizations of all samples s and their (dimensionless) Koenigsberger Q ratios (Koenigsberger, 1938) were determined based on the standard formula

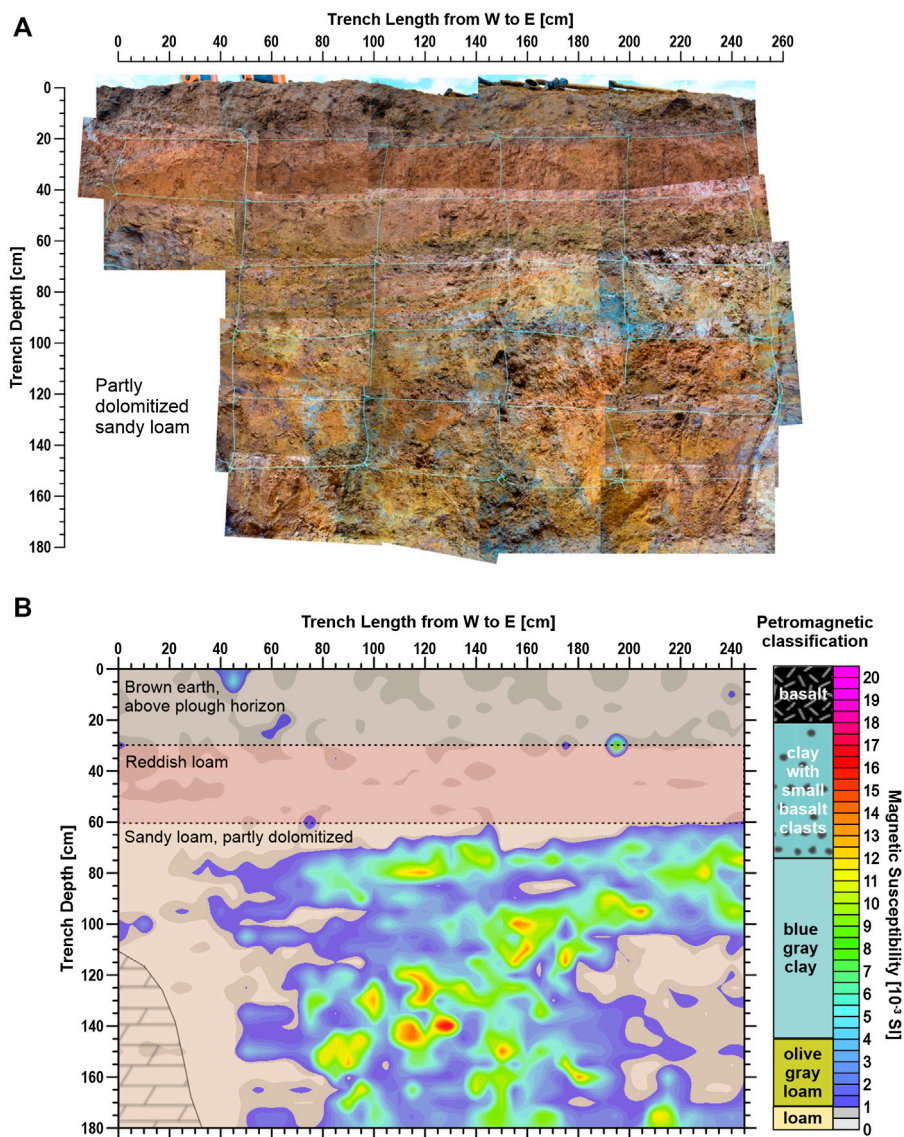


FIGURE 2 | (A) Photo mosaic of exploration trench wall with strings marking 25 × 50 cm sectors. The dolomitized sandstone in the lower left was later removed and measured, but not photographed. **(B)** Schematic host soil sections with overlain magnetic susceptibility contour plot based on *in-situ* susceptometry data collected on a 5 × 5 cm grid. Low-magnetic host rock soils (0–1 × 10⁻³ SI, gray) show pedoturbated fringes with the ochre and olive-gray medium-magnetic (1–4 × 10⁻³ SI, dark to light blue) and blue-gray high-magnetic (4–16 × 10⁻³ SI, green to yellow) basaltic weathering products. In 60 to 110 cm depth, basalt-derived clays are laterally protracted. The petromagnetic classification and color scheme at right associates basalt weathering stage with *in-situ* magnetic susceptibility.

$$Q(s) = \frac{M_{rem}(s)}{M_{ind}(s)} = \frac{NRM(s)}{\kappa(s) \cdot B/\mu_0}$$

RESULTS

Magnetic Anomaly Patterns and Burial Depth Estimates

At first glance, most ground magnetic W-E profiles (Figure 1B) remind on textbook-style anomalies of thin vertical dikes with soil or sediment overburden (Telford et al., 1990; Hinze et al.,

2013). Each of these profiles features a single central anomaly maximum of 60–160 nT amplitude dropping off to the local background without obvious side minima. These anomalies are perfectly aligned and trace the course of one single, straight, narrow, near-vertical volcanic dike with a length of ~1.5 km and a “Rhenish” strike of N8°E, intersected by two sinistral and one dextral *en échelon* offsets (Figure 1A).

However, at closer inspection, most of the observed anomalies display a greater range of shapes than theoretical “vertical sheet” anomaly formulas (Telford et al., 1990) can assume. Most peaks have single- or double-sided shoulders and/or tails of varying extent, some are crested with smaller spikes (<5 nT). These

irregular and diverse anomaly features within and beyond the dike section of **Figure 1B** imply, that additional magnetically enhanced material must exist at one or both sides of the dike. As these “abnormal” anomaly features are recorded with lower amplitudes at the upper magnetometer sensor and show a considerable short-range variability, they must relate to shallow (sub) soil structures.

Graphical depth estimation methods exploit the easily demonstrable circumstance, that overburden increases the half-width and straight slope length of a dike’s magnetic anomaly (e.g., Skilbrei 1993; Hinze et al., 2013). Testing various established methods, the most consistent and conclusive burial depths were obtained from the so-called “Sokolov Length” (Sokolov 1956). Under the assumption of a ~1 m wide buried dike, our Sokolov depth estimates (**Figure 1B**) declined from 2.5–1.7 m just below a hilltop situation in the southern part down to 0.9–0.5 m along a steepening valley slope in the northern part, which may reflect local equilibria of soil formation and soil erosion.

Soil Profile and Magnetic Susceptibility Map of Exploration Trench Section

The exploration trench was deliberately dug at a position where the dike is oblique to the hillslope and seemed to be only moderately buried (**Figure 1B**). A brown, well-mixed (“ploughed”) Ap topsoil reached down to a depth of ~30 cm (**Figure 2A**), which was still largely frozen during our early March campaign time, but could be easily identified by its crumbly texture and high content of shredded crop fibers. Below followed a ductile, clay-rich (“vertic”) Bv subsoil layer of 30–40 cm thickness (**Figure 2A**). This reddish loam was thought to be a colluvial soil from a previously overlying reddish Keuper mudstone. The beige sandy loam encountered below at 60–70 cm depth forms the C horizon and appears to originate from the underlying Burgsandstein bedrock, a dolomitic arkose. Below ~110 cm depth, this material became too hard to be penetrated by spade, and a gasoline-powered breaker hammer had to be used to reach the final trench depth of 180 cm.

In the center of the trench and coinciding with the magnetic anomaly peak, relicts of a vertical dike appeared in ochre, olive-, and blue-gray hues underneath the overlying colluvial soil (**Figure 2A**). The original basalt was fully replaced by cohesive, easily penetrable clays. Enclosed, mm-sized basaltic fragments scattered in the blue-gray clay witnessed the parent rock. The basalt-derived soil showed signs of decimeter-scale pedoturbation and/or pseudo-gley dynamics. In 60–110 cm depth, i.e. below the ductile reddish loam and above the hard, dolomitized beige sandy loam, this confined clay body was laterally protracted in downhill direction (**Figure 2**). Its lateral extent, determined by auger probing, reached ~2.5 m away from the dike, equivalent to a creep distance of ~4 m in downslope direction.

Whereas these complex deformation structures were partly camouflaged by pedoturbation (**Figure 2A**), the susceptibility map resolved the exposed basaltic soils and their boundaries in impressive detail (**Figure 2B**). Topsoil and subsoil originating

from the Upper Triassic Burgsandstein host rock were as low-magnetic ($\sim 0.5 \times 10^{-3}$ SI) as to be expected, while the susceptibilities of the basalt-derived olive- ($\sim 1\text{--}4 \times 10^{-3}$ SI) and blue-gray clays ($4\text{--}12 \times 10^{-3}$ SI) evidenced far higher magnetic mineral contents. Local susceptibility maxima of up to 18×10^{-3} SI marked patches of highly weathered basalt fragments. Consistent associations of soil color and magnetic susceptibility enabled us to establish a tentative, strictly local petromagnetic classification scheme (**Figure 2B**) dividing the observed dike materials in four progressive weathering stages: 1) pristine massive basalt, 2) partly weathered basalt with residual rock clasts, 3) fully weathered blue-gray basaltic clay with small rock fragments, and 4) oxidized olive-gray basaltic soil or loam. For simplicity, the arkose host rock and overlying host soils with their negligibly low background magnetizations were jointly classified as “Burgsandstein.”

Analytical 2D Anomaly Model of Weathered and Deformed Dike

When comparing the observed burial depth of the weathered dike (0.6 m, **Figure 2B**) with our Sokolov depth estimate (1.7 m, **Figure 1B**), a large discrepancy not just of both values, but also of both methods becomes apparent. While the observed burial depth marks the contact between the colluvial host soil and the clay-weathered dike head, the Sokolov method primarily “sees” the deeper, better preserved and more strongly magnetized dike segments. To separate the specific expressions of soil overburden and basalt weathering for a dike’s magnetic anomaly, we combined the structural information gained from the exploration trench with zonally averaged rock magnetic property values (**Figure 3B**), creating a case-specific 2D model dike (**Figure 3A**), whose magnetic anomaly can be numerically calculated (**Figure 3C**). To keep this numerical 2D model manageable required certain simplifications, but the dimensions, geometry and lateral zonation of the excavated dike section are rather well represented.

Our initial 2D model dike (not shown) produced a higher and broader anomaly than shown by our field data, which, as we assumed, was probably caused by over-estimating the pristine basalt volume at depth. As we had observed lateral weathering of a similar basalt dike down to 10–20 m depth at a river bank outcrop NE of Manau, we provided our model dike also with increasingly weathered outer flanks above 30 m depth (**Figure 3A**). Another modelling problem was linked to the inherent assumption of anomaly models that all bodies are homogeneously magnetized. Any deformation and dislocation of soil volumes and rock clasts should, however, result in a certain directional scatter and partial internal cancellation of their NRM vectors. We considered this cancellation effect suggested by our observed NRM inclinations and declinations by reducing measured NRM values by 30–50%, while keeping the induced magnetization unchanged (M_{ind} always follows the ambient geomagnetic field!). This lowers the Koenigsberger Q ratios of remanent vs. induced magnetization (**Figure 3B**), but Q values still agree well with value ranges reported in literature (Koenigsberger, 1938; Clark and Emerson, 1991). Our final

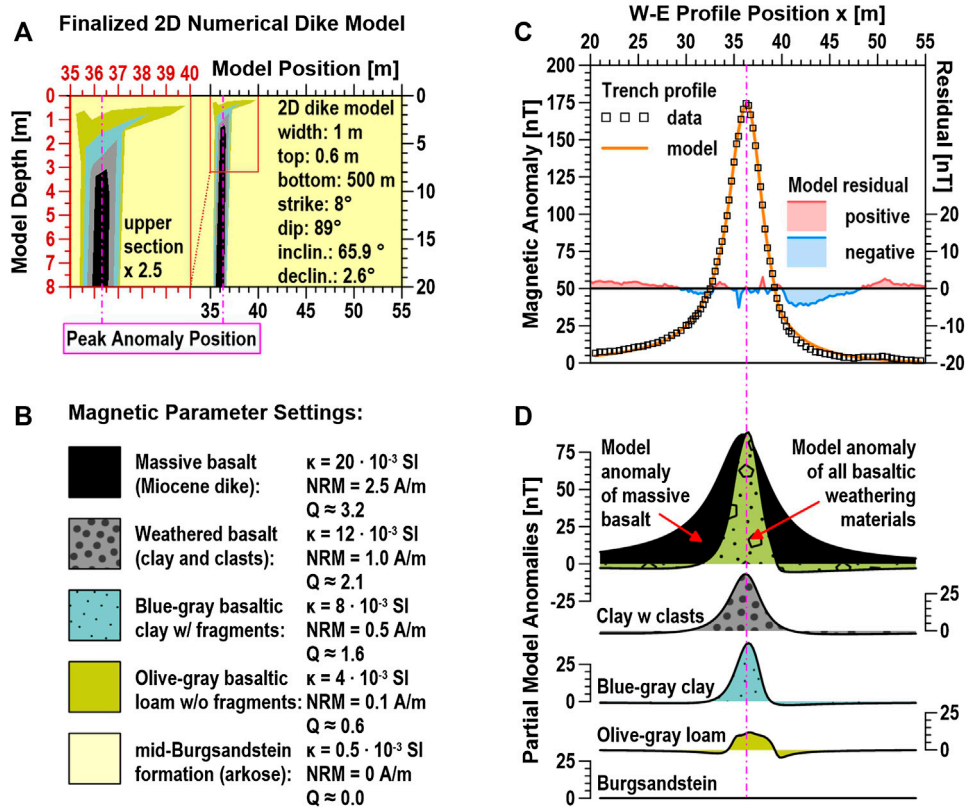


FIGURE 3 | (A) 2D model of weathered HDS dike based on the simplified and extrapolated exploration trench section of **Figure 2**. Shown at left (red axes) is a 2.5x enlarged view of the dike top; the smaller model at right (black axes) is scaled proportionally with **Figure 3C**. **(B)** Distinguished model materials, their color patterns and magnetic properties. **(C)** Total 2D dike model anomaly (orange line) and corrected ground magnetic survey anomaly data (squares) with model residuals (note vertical offset and expanded scaling of residual axis). **(D)** 2D model-based partial magnetic anomalies of pristine basalt (black), all weathering materials (olive green), and specific anomaly contributions by each material classified in **Figure 3B**. All anomaly axes are equivalently scaled in nT.

model has a Q of 3.2 for pristine basalt, which decreases to 2.1, 1.6, and 0.6 for the progressive weathering stages, reflecting a gradual loss of inherited thermoremanent and/or acquired chemical magnetization. A positive net magnetic anomaly at Q ratios >1 implies, that the basalt dike should have intruded and chilled during a period of a normally oriented geomagnetic field. Directional NRM data of the cube samples support this interpretation (see data in **Supplementary Material**).

With these justifiable geometry and parameter adjustments of the starting model, an excellent overall fit of modeled and observed magnetic anomalies was reached (note small model residuals in **Figure 3C**). The final model delivered not only a well-matching anomaly shape and amplitude, but also the formerly unknown contributions (i.e., “partial magnetic anomalies”) of all involved rocks and soils (**Figure 3D**). The pristine, semi-infinite basalt dike at depth creates a broad “vertical sheet” anomaly of ~8 m half-width. With its lesser depth and finite vertical extent, the weathered dike top generates a narrow “thick bed” anomaly (Eppelbaum, 2015) of ~3 m half-width with small, slightly asymmetric double-sided minima (**Figure 3D**). At this specific profile, the pristine basalt at depth contributes nearly 50% (86 nT) of the calculated peak anomaly (173 nT), while all basaltic weathering products together yield the remaining 50% (87 nT).

The W-E anomaly of this weathered dike model with N8°E strike and 88.9° dip features a slender central maximum with low, broad, slightly asymmetric, non-negative anomaly shoulders (**Figure 3C**) — a “composite” shape, that is typical for most HDS profiles (**Figure 1B**).

DISCUSSION AND CONCLUSION

Practical and Fundamental Insights From Our HDS Surveys

Ground magnetic surveying proved to be a reliable and efficient method to find and track weathered HDS dikes under meter-thick soil cover. Typical magnetic anomaly profiles across a buried HDS dike usually have a peak amplitude between 30 and 200 nT, but may occasionally reach 1,000 nT and more, when low-weathered basalt outcrops. We recognized that depth estimates from “Sokolov Length” and similar graphical methods provide just a relative guideline for the burial depth of clay-weathered dikes. Better depth estimates may be expected from specialized “weathered dike” models, whose control parameters include burial depth, weathering depth and dike top deformation. Creeping, slumping and blending of basaltic soil units within a

host soil complex can add tails, side peaks and troughs to the main dike anomaly (**Figure 1B**). Such complex and irregular anomaly patterns probably overstrain the adaptability of any parametrized inverse modelling approach and will always require forward anomaly modelling based on representative soil probing and a realistic starting model.

While pedogenesis converts a basalt's magmatic silicate minerals to clays, primary (titano-)magnetite is initially just oxidized to the likewise ferrimagnetic Fe mineral (titano-)maghemite (Cui et al., 1994; Garcia de Oliveira et al., 2002; Chen et al., 2005; Zhang et al., 2020). Basalt-derived clays thereby inherit large parts of their parent rock's magnetic minerals along with their strong induced and remanent magnetization. This circumstance explains the surprisingly high magnetization and excellent magnetic detectability of weathered dikes. As basalt weathering continues, this (Ti-)maghemite plus the iron released from weathered silicate minerals transform into secondary hematite and goethite (Lu et al., 2008). These antiferromagnetic minerals have far lower magnetizations, but lend their characteristic red and yellow colors to the ochre/olive-gray limonitic loam. *In-situ* susceptibility of weathered dikes is therefore an efficient method to visualize and map basalt weathering stages and soil creep in great detail. The contrasting colors and susceptibilities of basalt-derived marker soils are easy to follow along their deformation trajectory. Along-track mixing of basaltic and ambient soils should be quantifiable by linear magnetic unmixing based on endmember material properties (Heslop, 2015; Leng et al., 2019). As digging trenches in greater numbers and dimensions may get impractical, low-invasive, small-bore soil susceptometers as described by Petrovsky et al. (2004) could simplify *in-situ* susceptibility of larger soil sections and avoid unnecessary land damage.

Benefit of Basalt-Derived Marker Soils for Geomorphological Investigations

The diversity of magnetic anomaly shapes observed in this and other similar HDS surveys suggests, that old creep and slump structures underneath a usually well-mixed topsoil are very common (**Figure 1B**). The chosen exploration trench site represents a clear, but still modest case of soil deformation and creep. We found the most deviant magnetic anomalies predominantly at locations, where slope gradients were steeper and at larger angles with dikes, particularly in soil failure or confluence zones (**Figure 1B**). Counter-intuitively, basalt exhumed in our exploration trenches was typically more deeply weathered than the adjacent sandstone host rock. Where anomalies were locally large and narrow, this was always indicative of surficial low-weathered basalt related to topographically enhanced denudation or past human impact such as historical landscape terracing. Anomaly-based depth estimates necessarily overestimate the overburden of the weathered dike top and underestimate the depth of the pristine basalt. The spatial distribution of these numbers is nevertheless very useful to determine systematic and

frequently observable relative changes in soil cover, e.g., between hillcrest, hillslope and valley-floor, or between unworked (forests), pastured (meadows) and cultivated soils (cornfields).

Noticeably, our student surveys in the HDS region pursued geophysical and not geomorphological aims and provide just a pilot study for the proposed method. A dedicated soil creep study would e.g., include geotechnical soil properties and soil mechanics. Our findings can nevertheless illustrate the feasibility and validity of the depicted combined ground and rock magnetic dike mapping approach, that permits to find, map and diagnose the deformation of clay-weathered dike tops in continuity through changing terrain. Dike swarms like the HDS are globally abundant and transect different landscapes types parallel to crustal fracture systems. Their structural uniformity and good magnetic detectability make weathered dikes attractive as cross-temporary witnesses of soil deformation and delocalization under the joint influence of topography, bed-rock geology, pedogenesis, climate, vegetation and land use.

DATA AVAILABILITY STATEMENT

The original contributions presented in the study are included in the article/**Supplementary Material**, further inquiries can be directed to the corresponding author.

AUTHOR CONTRIBUTIONS

TD guided field courses, wrote the manuscript and designed or revised figures. MM and BB carried out the field work, performed laboratory measurements and processed and analyzed data for their MSc resp. BSc thesis. AK co-supervised the thesis projects as petrologist and regional expert. All coauthors actively contributed to the manuscript with ideas and comments.

ACKNOWLEDGMENTS

We greatly enjoyed the fabulous hospitality of Franconian country folks, who never bothered about our trespassing of their farmlands and readily shared their own observations on soil behavior with us. We wouldn't know the true course of any HDS dike without the highly committed field work of so far 120 field class participants. Two reviews and previous critical comments by Helge Stanjek helped us to substantially improve this manuscript and are gratefully acknowledged.

SUPPLEMENTARY MATERIAL

The Supplementary Material for this article can be found online at: <https://www.frontiersin.org/articles/10.3389/feart.2020.592986/full#supplementary-material>.

REFERENCES

- Abratis, M., Viereck, L., Pfänder, J. A., and Hentschel, R. (2015). Geochemical composition, petrography and $^{40}\text{Ar}/^{39}\text{Ar}$ age of the Heldburg phonolite: implications on magma mixing and mingling. *Int. J. Earth Sci.* 104, 2033–2055. doi:10.1007/s00531-015-1207-x
- Alestalo, J. (1971). Dendrochronological interpretation of geomorphic processes. *Fennia*. 105, 1–140.
- Chen, T. H., Xu, H. F., Xie, Q. Q., Chen, J., Ji, J. F., and Lu, H. Y. (2005). Characteristics and genesis of maghemite in Chinese loess and paleosols: mechanism for magnetic susceptibility enhancement in paleosols. *Earth Planet Sci. Lett.* 240, 790–802. doi:10.1016/j.epsl.2005.09.026
- Clark, D. A., and Emerson, D. W. (1991). Notes on rock magnetization characteristics in applied geophysical studies. *Explor. Geophys* 30, 547–555. doi:10.1071/EG991547
- Cui, Y., Verosub, K. L., and Roberts, A. (1994). The effect of low-temperature oxidation on large multi-domain magnetite. *Geophys. Res. Lett.* 21, 757–760. doi:10.1029/94GL00639
- Eppelbaum, L. V. (2015). Quantitative interpretation of magnetic anomalies from thick bed, horizontal plate and intermediate models under complex physical-geological environments in archaeological prospection. *Archaeol. Prospect.* 22, 255–268. doi:10.1002/arp.1511
- Garcia de Oliveira, M. T., Formoso, M. L. L., Indio da Costa, M., and Meunier, A. (2002). The titanomagnetite to titanomaghemite conversion in a weathered basalt profile from southern Paraná Basin, Brazil. *Clay Clay Miner.* 50, 478–493. doi:10.1346/000986002320514208
- Gärtner, H., and Heinrich, I. (2013). “Dendrogeomorphology,” in *Encyclopedia of quaternary science*. Editor S. A. Elias (Amsterdam, Netherlands: Elsevier B.V.), Vol. 2, 91–103. doi:10.1016/B978-0-444-53643-3.00356-3
- Geyer, G., and Schmidt-Kaler, H. (2006). *Die Haßberge und ihr Vorland: Wanderungen in die Erdgeschichte*. (Munich, Germany: Verlag Dr. Friedrich Pfeil), Vol. 20.
- Heslop, D. (2015). Numerical strategies for magnetic mineral unmixing. *Earth Sci. Rev.* 150, 256–284. doi:10.1016/j.earscirev.2015.07.007
- Hinze, W. J., von Frese, R. R. B., and Saad, A. H. (2013). *Gravity and magnetic exploration—principles, practices, and applications*. Cambridge, UK: Cambridge University Press.
- Johnson, D. L. (2002). Darwin would be proud: bioturbation, dynamic denudation, and the power of theory in science. *Geoarchaeology* 17, 7–40. doi:10.1002/geo.10001
- Koenigsberger, J. G. (1938). Natural residual magnetism of eruptive rocks. *Terr. Magnetism Atmos. Electr.* 43 (3), 299–320.
- Leng, W., von Dobeneck, T., Just, J., Govin, A., St-Onge, G., and Piper, D. J. W. (2019). Compositional changes in deglacial red mud event beds off the Laurentian Channel reveal source mixing, grain-size partitioning and ice retreat. *Quat. Sci. Rev.* 215, 98–115. doi:10.1016/j.quascirev.2019.04.031
- Lu, S.-G., Xue, Q.-F., Zhu, L., and Yu, J.-Y. (2008). Mineral magnetic properties of a weathering sequence of soils derived from basalt in Eastern China. *Catena*. 73, 23–33. doi:10.1016/j.catena.2007.08.004
- Mullender, T., Frederichs, T., Hilgenfeldt, C., de Groot, L., Fabian, K., and Dekkers, M. (2016). Automated paleomagnetic and rock magnetic data acquisition with an in-line horizontal “2G” system. *G-cubed*. 17, 3546–3559. doi:10.1002/2016GC006436
- Pawlik, Ł., and Šamonil, P. (2018). Soil creep: the driving factors, evidence and significance for biogeomorphic and pedogenic domains and systems—a critical literature review. *Earth Sci. Rev.* 178, 257–278. doi:10.1016/j.earscirev.2018.01.008
- Petrovsky, E., Hulka, Z., and Kapicka, A. (2004). A new tool for *in situ* measurements of the vertical distribution of magnetic susceptibility in soils as basis for mapping deposited dust. *Environ. Technol.* 25, 1021–1029. doi:10.1080/09593332508618391
- Pfänder, J. A., Jung, S., Klügel, A., Münker, C., Romer, R. L., Sperner, B., et al. (2018). Recurrent local melting of metasomatised lithospheric mantle in response to continental rifting: constraints from basanites and nephelinites/melilitites from SE Germany. *J. Petrol.* 59, 667–694. doi:10.1093/petrology/egy041
- Schröder, B. (1976). *Geologische Karte von Bayern, Blattnummer 5829 Hofheim: Bayerisches Landesamt für Umwelt*. (München, Germany: Scale 1:25,000).
- Skilbri, J. R. (1993). The straight-slope method for basement depth determination revisited. *Geophysics* 58, 593–595. doi:10.1190/1.1443442
- Sokolov, K. P. (1956). *Geological interpretation of magnetosurvey data*. Moscow, Russia: Gosgeoltechizdat, [in Russian].
- Telford, W. M., Geldart, L. P., and Sheriff, R. E. (1990). *Applied geophysics*. Cambridge, UK: Cambridge University Press.
- Wilson, M., and Downes, H. (2006). “Tertiary-Quaternary intraplate magmatism in Europe and its relationship to mantle dynamics,” in *European lithosphere dynamics*. Editors D. G. Gee and R. A. Stephenson (London, UK: Geological Society Memoirs), Vol. 32, 147–166.
- Zhang, Q., Appel, E., Stanjek, H., Byrne, J. M., Berthold, C., Sorwat, J., et al. (2020). Humidity related magnetite alteration in an experimental setup. *Geophys. J. Int.* 224, 69–85. doi:10.1093/gji/ggaa394

Conflict of Interest: The authors declare that the research was conducted in the absence of any commercial or financial relationships that could be construed as a potential conflict of interest.

Copyright © 2021 von Dobeneck, Müller, Bosbach and Klügel. This is an open-access article distributed under the terms of the Creative Commons Attribution License (CC BY). The use, distribution or reproduction in other forums is permitted, provided the original author(s) and the copyright owner(s) are credited and that the original publication in this journal is cited, in accordance with accepted academic practice. No use, distribution or reproduction is permitted which does not comply with these terms.